JOC The Journal of Organic Chemistry

Article

pubs.acs.org/joc

Origin of Asymmetric Induction in Bicyclic Guanidine-Catalyzed Thio-Michael Reaction: A Bifunctional Mode of Lewis Acid-Brønsted Acid Activation

Bokun Cho, Choon-Hong Tan, and Ming Wah Wong*

Department of Chemistry, National University of Singapore, 3 Science Drive 3, Singapore 117543

Supporting Information

ABSTRACT: In addition to a bifunctional Brønsted acid activation mode, an unconventional bifunctional mode of Lewis and Brønsted acid activations was revealed in a DFT study of bicyclic guanidine-catalyzed thio-Michael reaction. This activation mode provides an alternate reaction pathway for the C−S bond forming step and influences the final stereochemical outcome. The calculated turnover frequencies of the *R*- and *S*-products, based on the energetic span model, are in good accord with the observed high stereoselectivity toward the *S*-product.

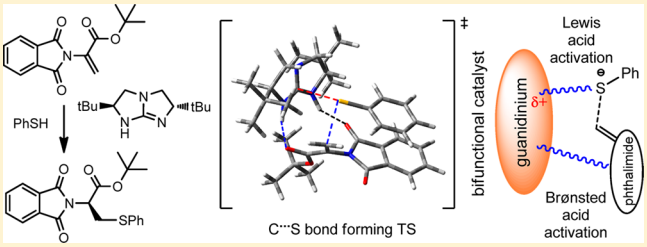

INTRODUCTION

Guanidines are well-known as Brønsted base catalysts for a wide variety of reactions.[1] The bifunctionality of guanidinium cation, the conjugate acid of guanidine, was initially proposed by Corey and Grogan for the asymmetric Strecker reaction.[2] This bifunctional activation mode, via simultaneous activation of both nucleophile and electrophile of the reactive partners through hydrogen bonding interactions, was supported by DFT calculations.[3] Through experimental and theoretical studies of Michael reaction,[4,5] we have further established the bifunctionality of bicyclic guanidinium ion. Independently, Jacobsen and co-workers utilized Brønsted acid activation of guanidinium in Claisen rearrangement.[6] It is important to note that guanidinium salts are used extensively in phase-transfer catalysis.[7] Nucleophilic activation via the Lewis basicity of guanidine provides an alternative activation mode, e.g. in ring-opening polymerization of cyclic esters[8] and intramolecular aldol reaction.[9] However, a bifunctional activation involving hydrogen bonding is slightly favored in the ring-opening polymerization reaction.[8]

The use of guanidinium ion as Lewis acid catalyst is relatively unknown. One rare example is the use of hexaalkyl guanidinium halide to catalyze epoxide ring-opening esterification, lactide ring-opening polymerization and decomposition of alkyl formate.[10] These authors proposed that the main mode of interaction is Lewis acidity. Experimental evidence of this type of activation mode is lacking. On the other hand, "Lewis acid interaction" via the central carbon atom of bicyclic guanidinium can be observed in X-ray crystal structures (Figure 1).[11] The central carbon of the guanidinium ion is strongly electrophilic (NBO charge +0.74; see the Results and Discussion section). Hence, a Lewis base (nucleophile) is expected to interact favorably with the highly electron deficient carbon of guanidinium ion. Here, we define "Lewis acid interaction" as an interaction between the electrophilic carbon of guanidinium and a nucleophile. On the basis of our crystal structure search on bicyclic guanidinium systems, five examples[11] of Lewis acid interaction were found, with interaction distance less than the sum of van der Waals radii. Here, we highlight three cases. In the dimer of Nb(H-hpp)Cl_4,[11a] the intermolecular interaction is achieved solely through Lewis acid interaction of the guanidine moiety, with C···Cl interaction distance of 3.26 Å (Figure 1). The X-ray structures of lasalocid acid with 1,5,7-triazabicyclo[4.4.0]-

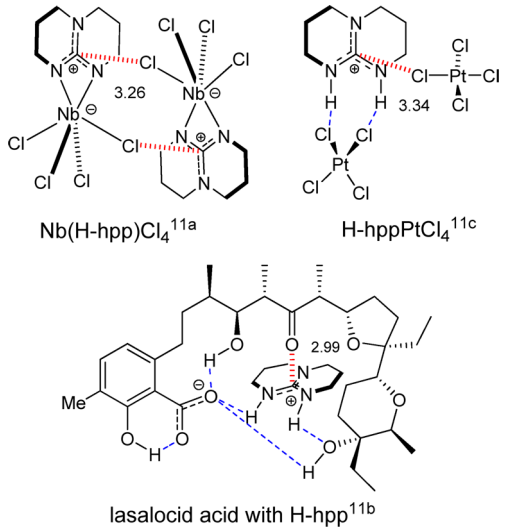

Figure 1. Three examples of crystal structure of bicyclic guanidinium system with "Lewis acid interaction". Interaction distances are given in Å.

Received: June 5, 2012
Published: July 12, 2012

   dx.doi.org/10.1021/jo301158c | *J. Org. Chem.* 2012, 77, 6553−6562

dec-5-ene (TBD or H-hpp) demonstrates that both Lewis acid and Brønsted acid interactions can occur simultaneously.[11b] In this case, both the hydroxyl and carboxylate groups are hydrogen bonded to the guanidinium N−H protons, while the ketone, acting as a Lewis base, interacts with the strongly Lewis acidic carbon of H-pp. Similar Lewis acid interaction is also revealed in the crystal structure of $(H\text{-hpp})_2PtCl_4$ complex.[11c] A chloride atom of one $PtCl_4$ unit serves as a Lewis base, while two chloride atoms of another $PtCl_4$ unit act as Brønsted bases (Figure 1). It is important to note that the Lewis acid interaction is more common in acyclic guanidinium. Hundreds of examples of C···Cl, C···Br and C···S interactions were found in our crystal database search.

We have previously reported that chiral bicyclic guanidine catalyzes the tandem thio-Michael−protonation reaction with high enantioselectivity (Scheme 1).[12] This catalytic reaction

Scheme 1. Bicyclic Guanidine-Catalyzed Tandem Thio-Michael−Enantioselective Protonation

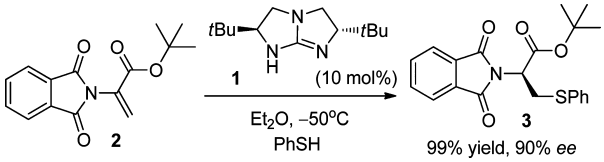

provides an effective method to prepare optically pure analogues of cysteine. In this paper, we investigated the catalytic mechanism and origin of enantioselectivity of the guanidine-catalyzed thio-Michael reaction (Scheme 1) using DFT method. Our calculations reveal an unconventional bifunctional activation of guanidinium, which serves simultaneously as a Lewis acid, via the electrophilic central carbon, and a Brønsted acid. This intriguing bifunctional mode of activation leads to an alternate reaction pathway that strongly influences the stereochemical outcome of the final product.

COMPUTATIONAL METHODS

Equilibrium structures and transition states (TSs) were fully optimized using the M06−2X[13] density functional method together with the 6-31G* basis set. The M06−2X functional was chosen, as this empirical functional is better suited than normal hybrid DFT methods (e.g., B3LYP) in handling kinetics, thermodynamics, and noncovalent interactions such as $\pi\cdots\pi$ interaction.[5,13,14] Frequency analyses were performed on the M06−2X/6-31G* optimized geometries to confirm the nature of the stationary points as equilibrium structures (with all real frequencies) or transition states (with only one imaginary frequency). The effect of solvation was examined by the SMD[15] implicit solvation model through M06−2X/6-311+G** single-point calculation, based on the gas-phase M06−2X/6-31G* optimized geometry. Both electrostatic and nonelectrostatic terms are included in the solvation calculations. Unless otherwise noted, the relative energies reported in the text correspond to relative free energies at 233 K (ΔG_{233}), computed at M06−2X/6-311+G**//M06−2X/6-31G* level in diethyl ether solvent. Charge density analysis was performed using the natural bond orbital (NBO)[16] approach based on the M06−2X/6-31G* wave function. DFT benchmarking calculations on representative transition states were performed using the 6-311+G** basis set with SMD solvation method, based on the M06−2X/6-31G* optimized geometries. All calculations were performed using the *Gaussian* 09 suite of programs.[17] The turnover frequencies were computed by the AUTOF program based on the energetic span model.[18] Crystal structure search was carried out using the Cambridge Structural Database.[19]

RESULTS AND DISCUSSION

Lewis Acid Interaction of Guanidinium Ion. It is instructive to first examine the Lewis acid interaction of guanidinium ion. On the basis of NBO analysis, the central carbon of the bicyclic guanidinium ion (**1**-H^+) is the most electrophilic atom (+0.74). The surrounding 3 nitrogen atoms are strongly negatively charged (Figure 2). The electrophilicity of

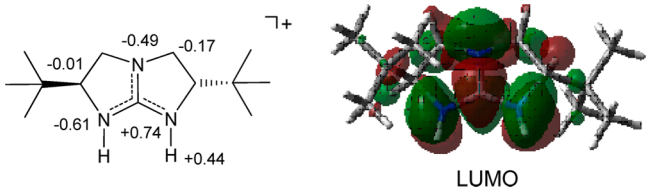

Figure 2. NBO atomic charges and the lowest unoccupied molecular orbital (LUMO) of the bicyclic guanidinium ion (**1**-H^+).

the central carbon is also reflected in the lowest unoccupied molecular orbital (LUMO), which is characterized by a vacant *p* orbital of the central carbon (see Figure 2). The strongly electrophilic carbon can readily complex with a nucleophile, particularly an anion. Thus, we envisaged a new bifunctional mode of guanidinium via the Lewis acidic carbon and the Brønsted acidic N−H protons simultaneously. Bicyclic guanidinium·$(Cl^-)_2$ complex (**1**-H^+·$(Cl^-)_2$, Figure 3) provides a simple model of this bifunctional mode of interactions. As evidenced in the optimized geometry (Figure 3), one chloride ion forms a bidentate hydrogen bond (2.24 Å) with both N−H protons, while the other chloride ion interacts with the Lewis acid guanidinium carbon, with an interaction distance of 3.30 Å. Indeed, a somewhat similar bifunctional mode is observed in the X-ray structure of a chloride complex of 6-membered ring bicyclic guanidinium.[11b] In this case, the C···Cl interaction (3.78 Å) is found between the guanidinium ion and a chloride anion of an adjacent molecule. For guanidinium·$(Cl^-)_2$, the calculated binding free energy (M06−2X/6-311+G**//M06−2X/6-31G*) of the second chloride ion is fairly large (−99 kJ mol^{-1}). Other strong nucleophile, such as RS^-, is expected to have similar magnitude of stabilization energy. Our DFT optimizations of the three examples of X-ray structure[11,20] confirm the Lewis acid type of interaction. The space filling models of these complexes show the close contact between the guanidinium carbon and nucleophile (Figure S1, Supporting Information).

Proposed Catalytic Mechanism. On the basis of previous theoretical studies of guanidine-catalyzed reactions,[4,5,6b,9] we envisaged three stages of the catalytic cycle (Scheme 2) for the reaction examined here: (1) deprotonation of thiophenol by the guanidine catalyst, (2) conjugate addition of thiophenolate ion to phthalimide to form an enolate intermediate, and (3) protonation of the enolate ion to yield the final product and regeneration of catalyst (**1**). The catalytic reaction is initiated by a facile proton transfer from thiophenol to the bicyclic guanidine catalyst, a superbase (e.g., pK_a of TBD = 22 in THF),[21] to form a hydrogen-bonded complex (**9**) between the guanidinium cation and thiophenolate ion. This ion-pair complex is characterized by a hydrogen bond between the guanidinium N−H proton and the sulfur atom of thiophenolate ion and N−H/π interaction between another N−H proton and the phenyl ring of thiophenolate. This complex has a binding free energy (ΔG_{233}, diethyl ether) of −8 kJ mol^{-1}. The calculated activation barrier

dx.doi.org/10.1021/jo301158c | J. Org. Chem. 2012, 77, 6553−6562

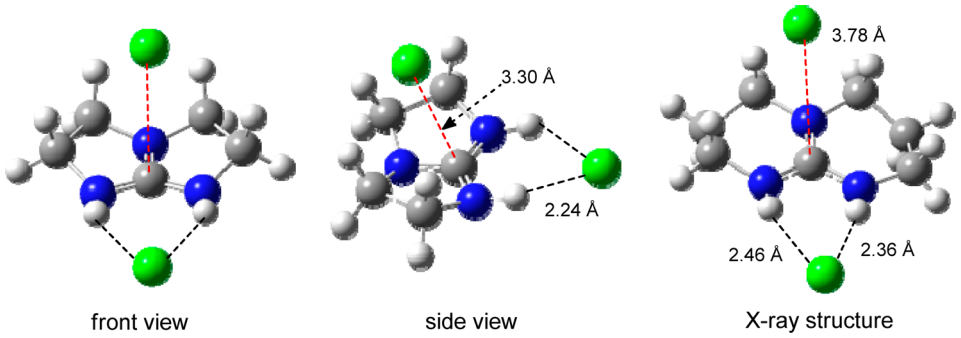

Figure 3. Optimized (M06−2X/6-31G*) geometry of bicyclic guanidinium·$(Cl^-)_2$ complex and a related X-ray structure.

Scheme 2. Schematic Reaction Pathways for Bicyclic Guanidine-Catalyzed Thio-Michael Conjugate Addition

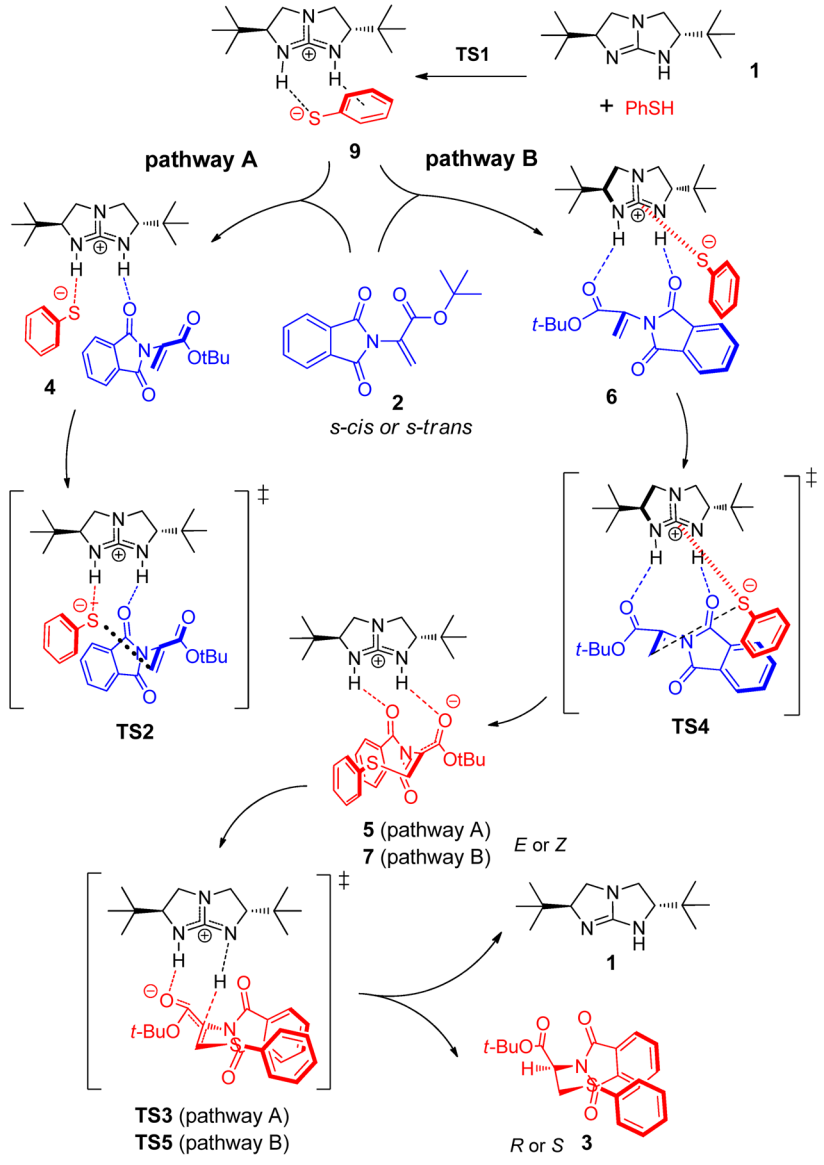

for this proton transfer process, via transition state **TS1**, is just 2 kJ mol^{-1}.

Phthalimide **2** exists in *s-cis* and *s-trans* forms, with respect to the conjugated alkene and ester functional groups. Both rotamers lie very close in energy, with the *s-trans* form slightly more stable by 3 kJ mol^{-1}. The *cis* and *trans* prefixes are used in subsequent related pre-TS complexes (**4** and **6**) and transition states (**TS2** and **TS4**) in the conjugate addition step to indicate clearly the conformation of the phthalimide moiety. Conjugate addition of thiophenolate ion to *s-cis*-**2** generates an *E*-enolate, while the *s-trans*-**2** leads to a *Z*-enolate (Scheme 3). The conjugate addition may proceed via two possible pathways (Scheme 2), namely, Brønsted acid activation (pathway A) and bifunctional Lewis and Brønsted acid activation (pathway B). The C−S bond forming

dx.doi.org/10.1021/jo301158c | J. Org. Chem. 2012, 77, 6553−6562

Scheme 3. Phthalimide 2 and Related Enolate Isomers

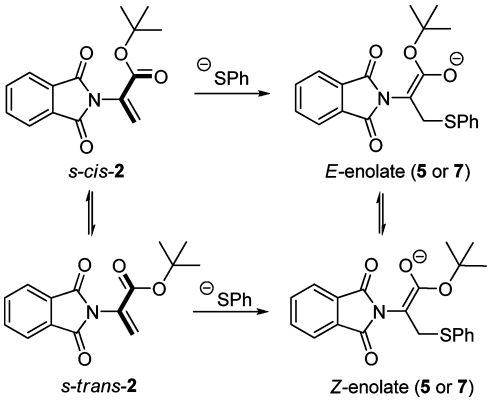

TS, enolate complexes and subsequent protonation TS associated with pathway A are labeled as **TS2**, **5** and **TS3**, respectively, while those related to pathway B are termed **TS4**, 7 and **TS5**, respectively (Scheme 2). The final protonation TS leading to a *S*- or *R*-product is indicated in the prefix of the TS (e.g., *R*-**TS3b**).

Pathway A: Brønsted Acid Activation. This type of bifunctional activation mode has been reported for other guanidine-catalyzed conjugate additions.[4,5] The conjugate addition is expected to proceed via a pretransition state complex **4**, characterized by dual hydrogen bonds between the reactants and guanidinium (Scheme 2). This complex plays a crucial role to assemble both substrates close to each other for the subsequent C−S bond formation. In pathway A, the bifunctional guanidinium catalyst serves as a Brønsted acid. This C−S bond forming step yields an enolate intermediate **5**, via transition state **TS2**. There are 5 possible ways of how the guanidinium catalyst can interact with both reactants simultaneously (Figure 4): monodentate hydrogen bonding to both thiophenolate ion and phthalimide (**2**) in **TS2a** and **TS2c**, bidentate hydrogen bonding to **2** and monodentate hydrogen bond to thiophenolate simultaneously in **TS2b**, and dual hydrogen bond to **2** only in **TS2d** and **TS2e**. Strictly speaking, **TS2d** and **TS2e** do not involve a bifunctional mode of activation since both guanidinium N−H protons do not interact with the thiophenolate substrate.

The optimized geometries of these 5 transition states (**TS2a**−**TS2e**) are shown in Figure 5. **TS2a**, **TS2b** and **TS2d** involve *s-trans*-**2**, while **TS2c** and **TS2e** relate to the *s-cis* isomer. Transition states with the *s-cis* conformation of phthalimide are energetically more favorable as they experienced less steric replusion and form stronger hydrogen bonds. This is supported by comparing of the hydrogen bond strength of *cis*-**TS2a** and *trans*-**TS2c** (Table S1, Supporting Information). The assembly of both reactants is required to induce the stereoselectivity. Bidentate hydrogen bond of both carbonyl groups from the ester and amide to a single acidic N−H of guanidinium in *trans*-**TS2b** stabilizes the TS more than that of monodentate hydrogen bond to the amide carbonyl group as shown in *trans*-**TS2a**. In addition, activation of the phthalimide **2** via dual hydrogen bonding with both acidic N−H of the guanidinium, namely *cis*-**TS5d** and *trans*-**TS2a** (Figure 5), can accommodate both the *s-cis* and *s-trans* conformations of **2**, and both *R* and *S* enantiomeric products can be formed through this mode of interaction.

The conjugate addition step, via **TS2**, yields an enolate complex **5**, with energy comparable to or slightly higher than pre-TS complex **4** (Figure 6). Protonation of the enolate intermediate, via **TS5**, leads to the final addition product (**3**). Interestingly, this protonation step has a significantly lower activation barrier than the C−S bond forming step for all reaction paths (a−e) considered (Figure 6). In other words, the C−S

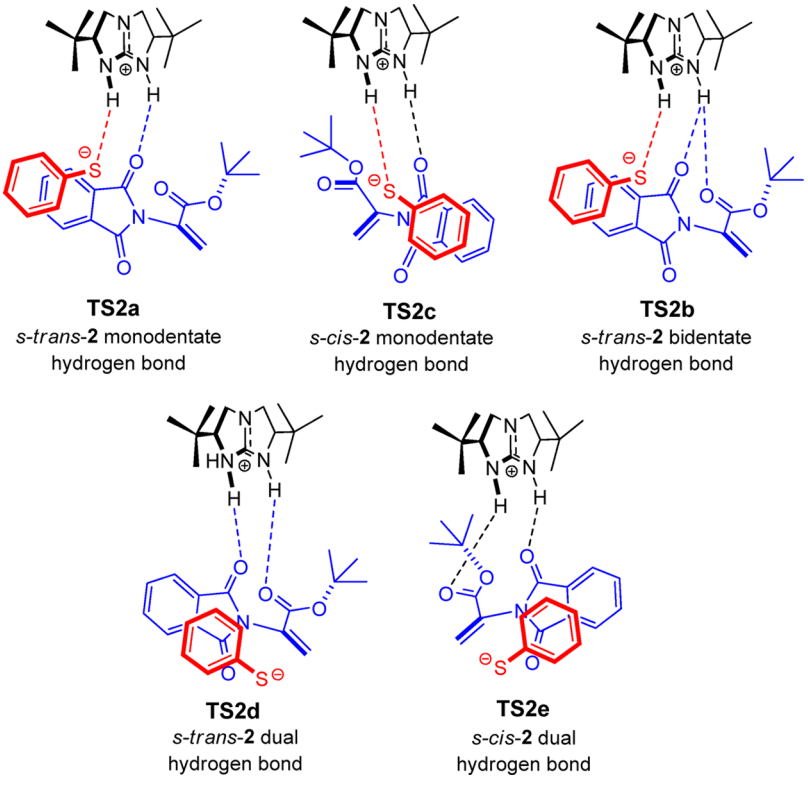

Figure 4. Five possible binding modes of the C−S bond forming transition state (**TS2a**−**TS2e**) of pathway A.

dx.doi.org/10.1021/jo301158c | *J. Org. Chem.* 2012, 77, 6553−6562

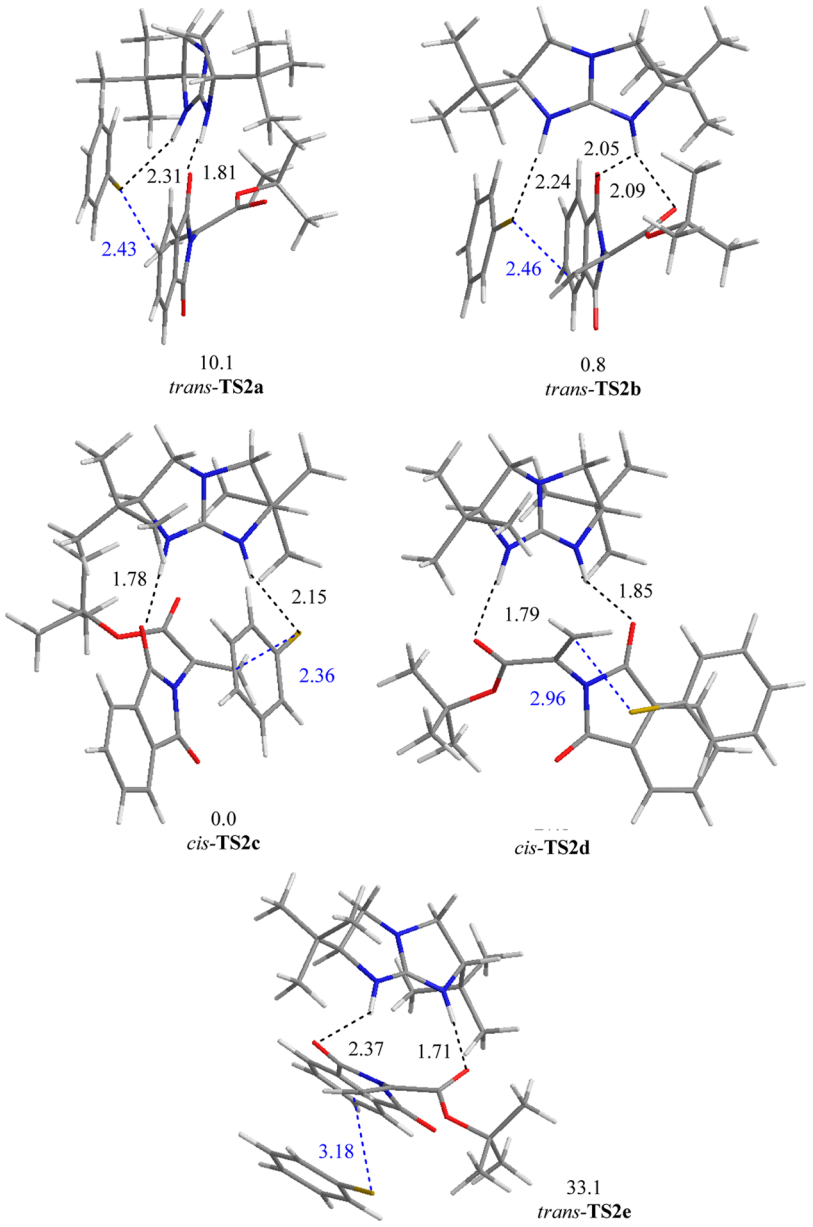

Figure 5. Optimized (M06−2X/6-31G*) geometries of various **TS2** transition states. Relative free energies (ΔG_{233} in diethyl ether, kJ mol^{-1}), relative to *cis*-**TS2c**.

bond formation is the rate-determining step for the Brønsted acid activation pathway. Overall, the activation barrier of this C−S bond forming step is rather low, with *s-trans*-**2** having a lower activation barrier than *s-cis*-**2**, 20 and 37 kJ mol^{-1}, via *trans*-**TS2b** and *cis*-**TS2c**, respectively (Figure 6). For the formation of the *R*-product, the representative path is *trans*-**4b** → *trans*-**TS2b** → *Z*-**5b** → *R*-**TS3b** (Figure 6) as it has significantly higher catalytic turnover frequency (see last section) compared to other energetic paths.

Pathway B: Bifunctional Lewis Acidic and Brønsted Acidic Activation. An alternate pathway, designated pathway B (see Scheme 2), is also expected on the basis of a plausible Lewis acid activation mode of the guanidinium carbon. In this case, the bifunctional catalyst serves simultaneously as a Lewis acid and a Brønsted acid. Since there are two hydrogen bond acceptors (i.e., oxygen atoms of amide and ester groups) in phthalimide, they could interact simultaneously with the guanidinium catalyst via dual hydrogen bonds. At the same time, C···S interaction is possible between guanidinium and thiophenolate via the Lewis acid interaction. Hence, a 3-point pretransition state complex **6** is expected for pathway B (Scheme 2). For *s-cis*-**2**, this form of substrate assembly yields a stable complex *cis*-**6a**, with a binding free energy of −48 kJ mol^{-1}. The optimized geometry of *cis*-**6a** confirms the hydrogen bond interactions with both carbonyl groups of the ester and amide moieties. On the other hand, dual hydrogen bond interactions of *s-trans*-**2** with guanidinium can only accommodate hydrogen bonding to the ether functionality of the ester and the carbonyl of the amide in the less stable *trans* complex (*trans*-**6d**). For the same reason, the C−S bond forming transition state *trans*-**TS4d** is 20 kJ mol^{-1} less stable than *cis*-**TS4a** (Figure 7). If *s-trans*-**2** forms dual hydrogen bonds via the carbonyl groups of the ester and the amide moieties, it will sterically hinder the thiolate to interact with the guanidinium catalyst through Lewis acidic interaction.

In pathway B, all the C−S bond forming transition states (**TS4a**−**TS4d**, Figure 7) are characterized by a close C···S

dx.doi.org/10.1021/jo301158c | J. Org. Chem. 2012, 77, 6553−6562

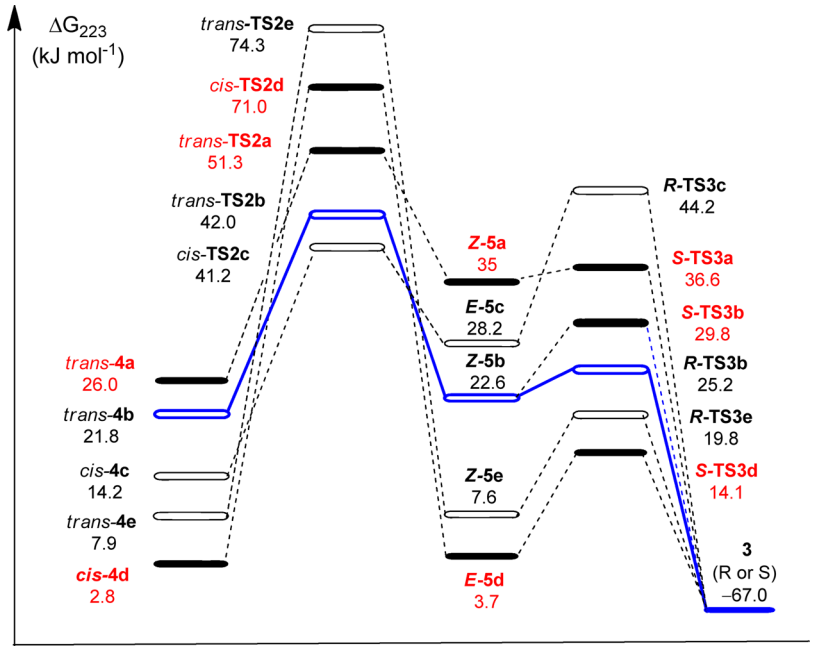

Figure 6. Schematic potential energy diagram of pathway A. Filled bars are the energetic pathways leading to *S*-product, while blank ones results in *R*-product. The pathway in bold is the representative path. Relative free energies (ΔG_{233} in diethyl ether solvent, kJ mol^{-1}) were calculated at M06−2X/6-311+G**//M06−2X/6-31G* level.

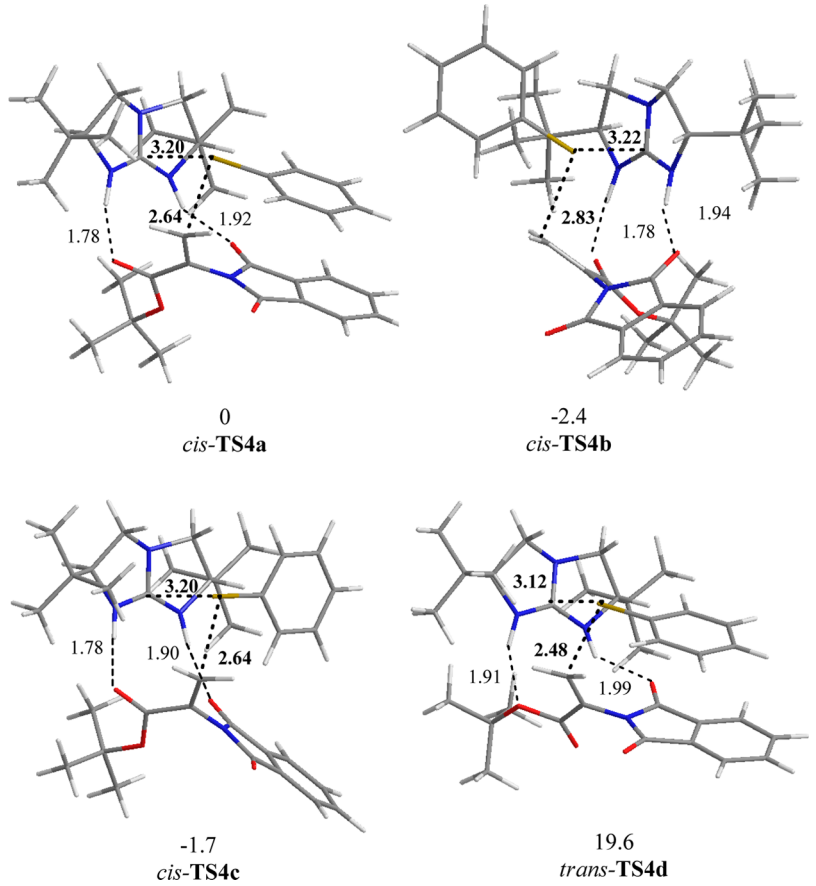

Figure 7. Optimized (M06−2X/6-31G*) geometries of various **TS4** protonation transition states. Relative free energies (ΔG_{233} in diethyl ether, kJ mol^{-1}), relative to *cis*-**TS4a**.

contact (3.12−3.22 Å) between the guanidinium carbon and thiophenolate sulfur. In addition, three types of interaction modes were observed for the various **TS4** transition states (Figure 7): (1) dual hydrogen bonding to both carbonyl groups of the amide and ester of **2** with $\pi\cdots\pi$ aromatic stacking between the thiophenolate and **2** in *cis*-**TS4a**, (2) dual hydrogen bonding

dx.doi.org/10.1021/jo301158c | *J. Org. Chem.* 2012, 77, 6553−6562

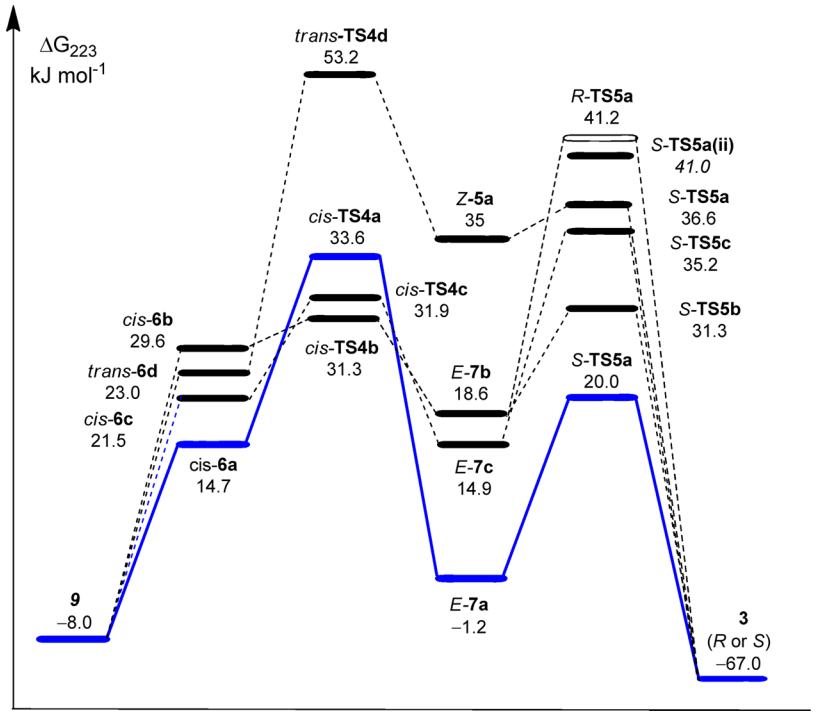

Figure 8. Schematic potential energy diagram of pathway B. Filled bars are the energetic paths leading to *S*-product, while blank one results in *R*-product. The pathway in bold is the representative path. Relative free energies (ΔG_{233} in diethyl ether solvent, kJ mol^{-1}) were calculated at M06−2X/6-311+G**//M06−2X/6-31G* level.

to amide and ester moieties with C−H···π interaction between the guanidinium C−H and the phenyl ring of thiophenolate in *cis*-**TS4b** and *cis*-**TS4c**, and (3) dual hydrogen bonding to the ether moiety of the ester and the carbonyl group of the amide with $\pi\cdots\pi$ aromatic stacking between the thiophenolate and **2** in *trans*-**TS4d**. It is worth noting that *trans*-**TS4d** and *trans*-**TS2a** share the same subsequent enolate complex and protonation pathway.

This alternate bifunctional activation mode (i.e., pathway B) allows *cis*-**6a** to access a kinetically more favorable route via transition state *cis*-**TS4** when compared to the C−S bond forming transition state (**TS2**) in pathway A, through pre-TS complex **4** (cf. Figures 6 and 8). The stronger catalyst activation is supported by the larger positive charge on the conjugated β carbon of the phthalimide moiety and the stronger negative charge on the sulfur atom of the thiophenolate moiety in *cis*-**TS4a**. The enhanced electrophilicity of **2** and enhanced nucleophilicity of thiophenolate anion leads to greater stabilization of *cis*-**TS4a** and, hence, a significantly lower C−S addition barrier of 18.9 kJ mol^{-1} for pathway B, via *trans*-**TS2b** (Figure 8). The importance of the Lewis acidic interaction can be seen in *cis*-**TS2d** and *trans*-**TS2e**, where the thiophenolate Lewis acidic interaction is absent despite the dual hydrogen bonding with the catalyst. Both *cis*-**TS2d** and *trans*-**TS2e** have a larger activation barrier, ~40 kJ mol^{-1} higher than that of *cis*-**TS4a**. In summary, pathway B provides a more efficient pathway to generate the *S*-product.

Interestingly, the chirality of the reaction product for pathway B is locked in the C−S bond forming step because of the strong ion-pair interaction between the guanidinium ion and the anionic substrates. As a consequence, protonation of enolate occurs in the same face as the conjugate addition step. It is worth noting that the strength of the guanidinium ion-pair interaction is frequently utilized in phase-transfer catalysis, where this favorable electrostatic interaction enables the reactants to shuttle between aqueous phase and organic phase.[7] Because of the steric constraint of the two bulky *t*-butyl groups of the bicyclic guanidinium catalyst, isomerization of the enolate intermediate is difficult in the catalyzed reaction. For comparison, the free enolate has an *E*−*Z* rotational barrier of 91 kJ mol^{-1}, while the enolate complex *E*-**7a** has a substantially higher *E*−*Z* rotational barrier of 167 kJ mol^{-1}. For the enolate complex **7**, the *E* form is considerably more stable than the *Z* form. In other words, the phthalimide moiety favors a *cis* conformation in the enolate complex **7**, in distinct contrast to the free form of phthalimide which slightly favors the *s-trans* conformation (by 3 kJ mol^{-1}).

There is little facial selectivity for both pathways A and B (see Figure S2, Supporting Information) for the catalyst as the orientation of the reactants remains more or less the same when phthalimide (**2**) approaches from either face. Pathway B only allows one orientation of the phthalimide to be complexed with the guanidinium catalyst. This orientation exposes the face that is the pro-*S* face of the resultant prochiral enolate from the C−S conjugate addition step. The subsequent enantioselective protonation step abstracts a proton from the same face, which yields the *S*-product. Because of the limited rotational freedom of the enolate complex (*E*-**7**) and the difficulty in accessing the proton from the opposite face, pathway B will yield the *S*-product almost exclusively, in sharp contrast to pathway A. The representative path of pathway B is *cis*-**6a** → *cis*-**TS4a** → *E*-**7a** → *S*-**TS5a** → *S*-**3** (Figure 8) since it has a considerably higher turnover frequency compared to other energetic paths (see the last Section).

Enolate Stability. The enolate intermediates are stabilized by complexation with the guanidinium catalyst. These complexes (**5** or **7**) are characterized by the same hydrogen bonding interactions as the preceding C−S bond forming transition states (**TS2** or **TS4**, respectively). For the enolate complexes that

dx.doi.org/10.1021/jo301158c | *J. Org. Chem.* 2012, 77, 6553−6562

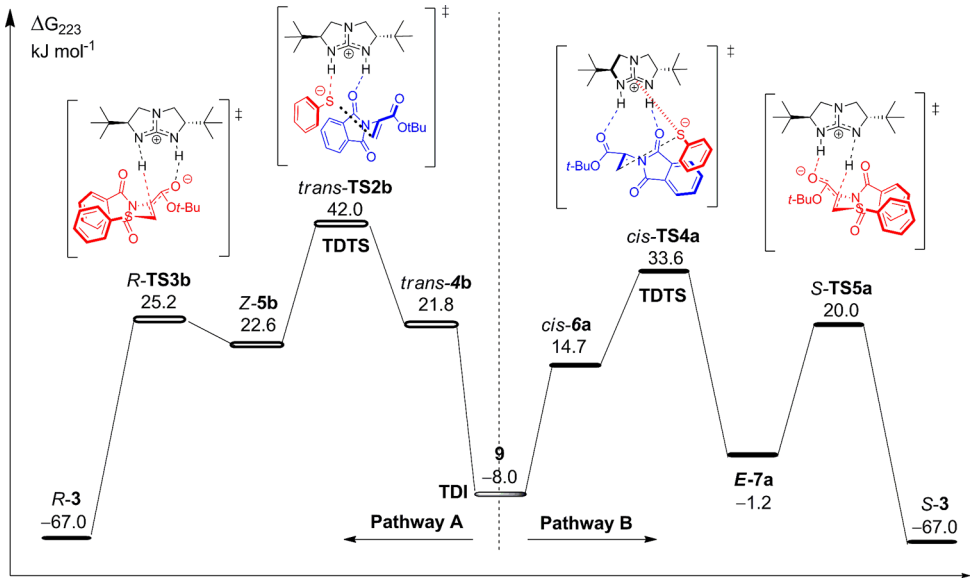

Figure 9. Schematic potential energy diagram showing the formation of the *R*- and *S*- products via pathways A and B, respectively. Calculated relative free energies (ΔG_{233}) at M06−2X/6-311+G**//M06−2X/6-31G* level (in diethyl ether).

possess hydrogen bonding to both carbonyl oxygens of the ester and amide moieties in the enolate complexes, namely, *E*-**5d**, *Z*-**5e**, *E*-**7a**, *E*-**7b**, and *E*-**7c**, they are more stable than those with monodentate hydrogen bonding to the enolate. This is attributed to the greater basicity of the carbonyl moieties that form such robust hydrogen bonds, which is readily supported by the hydrogen bond lengths and NBO donor−acceptor interactions, on the basis of second-order perturbation theory (Table S2, Supporting Information). Among the enolates with bidentate carbonyl hydrogen bonding, *E*-**5d**, *Z*-**5e**, and *E*-**7a** are significantly more stable because of additional π stacking interaction between the phthalimide and thiophenolate moieties.

Enantioselective Protonation Step. The enantioselectivity of the final product depends on whether the protonation occurs on the *Re* or *Si* face of the enolate in the enantioselective protonation step. For pathway B, protonation can only occur on the same face as the C−S bond forming step. Thus, the chirality of the reaction product is locked in the *cis*-**6** complex. In a somewhat similar manner, the geometry of the enolate intermediate will determine the preference of protonation for pathway A. Protonation from the opposite face requires uncomplexation of the fairly stable enolate-guanidinium complex, which has a binding free energy of −103 kJ mol^{-1} (for *E*-**7**). Furthermore, protonation TS from the opposite face is less stable because of steric constraints, as reflected in the TS energies of *R*-**TS5a** and *S*-**TS3b** (Figures 8 and 6, respectively). Hydrogen bonding to the carbonyl oxygen of enolate ester leads to more stable transition states. Comparison of *S*-**TS5a** and *R*-**TS3b** with *S*-**TS5a(ii)** (hydrogen bond to amide carbonyl) and *R*-**TS3a** (hydrogen bond to ester ether oxygen) confirms the energetic preference toward the ester carbonyl hydrogen bonding, which has the strongest Brønsted basic interactions.

It is worthwhile to note that $\pi-\pi$ stacking interaction between the phenyl ring of the thiophenolate and the anhydride moiety of phthalimide is an important stabilization interaction in the enolate intermediates, products as well as the protonation transition states. For instance, the conformation of the *S*-product without intramolecular $\pi-\pi$ interaction is significantly higher in the energy (by 18 kJ mol^{-1}) than the lowest-energy structure with favorable $\pi-\pi$ stacking interaction. In addition to the stabilizing effect on enolate, $\pi-\pi$ stacking makes the enolate more compact; optimizing the hydrogen bonding while minimizing steric hindrance with the catalyst as verified by the shorter hydrogen bond length and stronger NBO donor and acceptor interaction. The effect of $\pi-\pi$ aromatic ring stacking can be seen in the significant energetic stabilization of the protonation transition state *S*-**TS5a** over *S*-**TS5b** and *S*-**TS5c** (Figures S3 and S4, Supporting Information).

Enantioselectivity and Turnover Frequencies. Unlike typical reactions governed by the Curtin−Hammett principle, where a single rate-determining step determines the stereoselective outcome of the reaction, both the C−S bond forming and protonation steps of the catalytic reaction investigated here can influence the overall rate significantly (Figures 6 and 8). Pathway B provides a substantially lower activation barrier for the C−S bond formation step. However, the subsequent protonation TS is not necessarily lower in energy than the corresponding C−S bond forming TS (Figure 8). Hence, simply comparing the relative energies of various transition states of a particular step is not sufficient to elucidate the overall enantioselectivity. The energetic span model of Kozuch and Shaik[18,22] provides a more realistic approach to assess the kinetics by factoring in the energetic contributions of all the intermediates and transition states to the overall rate and turnover frequencies (TOFs). In this energetic span model, the TOF determining intermediates (TDI) and transition state (TDTS) are the states that affect the rate, and in turn the TOF, most significantly, and these states may be different for different reaction pathways. In the catalytic reaction examined here, the TDI is same for both pathways A and B, which is the thermodynamically most stable guanidinium-thiolate complex **9**. The TDTS is different for each reaction pathway. For the formation of the *S*-product via pathway B (Figure 9), the TDTS is *cis*-**TS4a**, which links to *E*-**7a**, *S*-**TS5a**, and finally to product *S*-**3**. On the other hand, *trans*-**TS2b** is the TDTS for pathway A, which leads to the *R*-product (*R*-**3**). It links to complex *trans*-**4b**, enolate *Z*-**5b** and protonation TS *R*-**TS3b** (Figure 9). Since TOF is defined as the number of catalytic cycles that a particular pathway can complete within a period of time, the magnitude correlates directly to the proportion of product produced. We can calculate the number of cycles obtained per

dx.doi.org/10.1021/jo301158c | J. Org. Chem. 2012, 77, 6553−6562

hour by each pathway (from both pathways A and B) leading to the *S*- or *R*-product. Hence, by comparing the ratio of the TOFs (Table S4, Supporting Information) of the *S*-product (by both pathways A and B) and *R*-product (by pathway A only), we can estimate the enantiomeric excess (ee) of the catalytic reaction studied here. On the basis of this approach, the formation of the *S*-product is predicted to be 100 times faster than the *R*-product. The predicted ratio is indeed in good accord with the observed preference for the *S*-enantiomer.[12] It is important to note that because of the strong kinetic preference toward the representative paths in both pathways A and B (Figures 6 and 8), the TOF contributions from other reaction paths are very small and, therefore, not included in the TOF calculations. In summary, the conjugate addition step of pathway B strongly influences the computed TOF. This readily demonstrates the importance of the alternate activation mode in controlling the stereoselectivity of the catalytic reaction.

Benchmarking of DFT Methods for Guanidinium Lewis Acidic Interaction. Because of the longer interaction distance of the Lewis acidic activation (approximately 3.2 Å in **TS4**) and the importance of $\pi\cdots\pi$ interaction in several intermediates and transition states, proper treatment of long-range dispersion in the DFT method employed is expected to be important. Thus, it is instructive to examine the performance of various DFT methods on the relative energies of several key transition states. To this end, we have chosen several popular hybrid DFT methods such as B3LYP[23] and PBE[24] and the dispersion corrected counterparts, namely B3LYP-D[25] and PBE-D,[25] as well as ω-B97X-D[26] functional. In these benchmark calculations, 6-311+G** basis set was employed, on the basis of M06−2X/6-31G* optimized geometries. Here, we compare the relative energies for several key transition states. Three representative transition states with different modes of activation for both the C−S bond forming step and their corresponding enantioselective protonation step were selected, which included pathways for both *R*- and *S*-products: (a) the most favorable pathway B route in the kinetics (*cis*-**TS4a** → *S*-**TS5a**); (b) the most favorable pathway A route (*trans*-**TS2b** → *R*-**TS3b**); and (c) the dual hydrogen bonded C−S bond forming TS without Lewis acidic activation in pathway A (*cis*-**TS2d** → *S*-**TS3d**).

As evidenced in Table 1, the dispersion corrected DFT methods, ωB97X-D, B3LYP-D, PBE-D, M06−2X, give the same trend for both the C−S bond forming and protonation steps, favoring the Lewis acidic activation pathway B. The absence of Lewis acidic and Brønsted activation on the thiophenolate in *cis*-**TS2d** makes it highly unstable in all 4 dispersion corrected DFT methods, in distinct contrast to the B3LYP and PBE results. For comparison, *trans*-**TS2b** is predicted to be the most favorable TS by B3LYP and PBE functional. In this case, both phthalimide and thiophenolate substrate are activated by hydrogen bonding, which is well described by the conventional DFT methods. For *cis*-**TS4a**, B3LYP and PBE predict that it is less stable than *trans*-**TS2b** because of its inadequate treatment for dispersion interaction. The requirement of proper treatment of dispersion for reliable prediction of relative energies is further confirmed by MP2 calculations with a smaller 6-31G* basis set. As expected, the dispersion corrected DFT methods correctly reproduce the trend of relative energies of various transition states calculated at the MP2 level.

All the DFT methods yield the same trend in the relative energies of the protonation transition states where only guanidinium hydrogen bonding activation is involved. This finding further demonstrates the importance of dispersion treatment for the long-range guanidinium Lewis acid activation.

Table 1. Benchmark Result of Relative Free Energies ($\Delta\Delta G^{\neq}$, kJ mol^{-1}) of Representative Thiol-Michael Transition States with Different DFT Methods[a,b]

transition state	M06−2X	ωB97X-D	B3LYP-D	PBE-D	B3LYP	PBE
cis-**TS4a**	0.0	0.0	0.0	0.0	0.0	0.0
trans-**TS2b**	8.4	10.5	7.9	1.3	−0.6	−13.6
cis-**TS2d**	37.4	37.0	32.9	31.1	5.6	11.6
S-**TS5a**	0.0	0.0	0.0	0.0	0.0	0.0
R-**TS3b**	5.2	1.6	7.0	7.6	23.2	19.2
S-**TS3d**	−5.9	−8.8	−7.8	−9.2	−13.4	−7.9

[a]All DFT methods were calculated with the 6-311+G** basis set using the SMD solvation method (in diethylether), based on M06−2X/6-31G* geometries. [b]The three protonation TSs in the last three rows are in the same order as their respective C−S bond forming TSs in the first three rows.

CONCLUSIONS

DFT calculations were employed to shed light on the catalytic mechanism and the origins of stereoselectivity of bicyclic guanidine catalyzed-thio-Michael reaction of thiophenol with phthalimide. In addition to the Brønsted acid bifunctional activation mode, an unconventional bifunctional activation of guanidinium, which serves simultaneously as a Lewis acid, via the electrophilic central carbon, and a Brønsted acid, is revealed in our computational study. This intriguing activation mode provides an alternative pathway of the catalytic reaction and critically influences the stereoselectivity of the thio-Michael addition product. The Lewis acid type of interaction of the guanidinium carbon is readily supported by several X-ray structures in literature. The selectivity for the *s-cis* phthalimide in pathway B and the strength of the guanidinium ion-pair interaction permit only the *Si* face to be attacked in both the C−S bond forming and enantioselective protonation steps. The calculated turnover frequencies, of both *R*- and *S*-products, based on the energetic span model, agrees well with the observed enantioselectivity. Dispersion treatment in DFT method is essential in proper description of the long-range "Lewis acid interaction" in guanidinium.

ASSOCIATED CONTENT

Supporting Information

Optimized geometries of key transition states, coordinates of all optimized geometries (in .xyz format, zip file), NBO charges and hydrogen bonding analysis of intermediates and transition states, and input of TOF calculations. This material is available free of charge via the Internet at http://pubs.acs.org.

AUTHOR INFORMATION

Corresponding Author

*E-mail: chmwmw@nus.edu.sg.

Notes

The authors declare no competing financial interest.

REFERENCES

(1) (a) Leow, D.; Tan, C.-H. *Chem.—Asian J.* **2009**, *4*, 488−507. (b) Leow, D.; Tan, C.-H. *Synlett* **2010**, *11*, 1589−1605. (c) Shen, J.; Nguyen, T. T.; Goh, Y. P.; Ye, W.; Fu, X.; Xu, J.; Tan, C.-H. *J. Am. Chem. Soc.* **2006**, *128*, 13692−13693. (d) Fu, X.; Jiang, Z.; Tan, C.-H. *Chem. Commun.* **2007**, 5058−5060. (e) Jiang, Z.; Ye, W.; Yang, Y.; Tan, C.-H.

Adv. Synth. Catal. **2008**, *350*, 2345−2351. (f) Jiang, Z.; Yang, Y.; Pan, Y.; Zhao, Y.; Liu, H.; Tan, C.-H. *Chem.—Eur. J.* **2009**, *15*, 4925−4930. (g) Liu, H.; Leow, D.; Huang, K. W.; Tan, C.-H. *J. Am. Chem. Soc.* **2009**, *131*, 7212−7213. (h) Terada, M.; Ikehara, T.; Ube, H. *J. Am. Chem. Soc.* **2007**, *129*, 14112−14113. (i) Terada, M.; Ube, H.; Yaguchi, Y. *J. Am. Chem. Soc.* **2006**, *128*, 1454−1455.

(2) Corey, E. J.; Grogan, M. J. *Org. Lett.* **1999**, *1*, 157−160.

(3) Li, J.; Jiang, W.-Y.; Han, K.-L.; He, G.-Z.; Li, C. *J. Org. Chem.* **2003**, *68*, 8786−8789.

(4) Jiang, Z.; Pan, Y.; Zhao, Y.; Ma, T.; Lee, R.; Yang, Y.; Huang, K. W.; Wong, M. W.; Tan, C.-H. *Angew. Chem., Int. Ed.* **2009**, *48*, 3627−3631.

(5) Cho, B.; Tan, C.-H.; Wong, M. W. *Org. Biomol. Chem.* **2011**, *9*, 4550−4557.

(6) (a) Uyeda, C.; Jacobsen, E. N. *J. Am. Chem. Soc.* **2008**, *130*, 9228−9229. (b) Uyeda, C.; Jacobsen, E. N. *J. Am. Chem. Soc.* **2011**, *133*, 5062−5075.

(7) (a) Hashimoto, T.; Maruoka, K. *Chem. Rev.* **2007**, *107*, 5656−5682. (b) Arai, S.; Tokumaru, K.; Aoyama, T. *Chem. Pharm. Bull.* **2004**, *52*, 646−648.

(8) (a) Chuma, A.; Horn, H. W.; Swope, W. C.; Pratt, R. C.; Zhang, L.; Lohmeijer, B. G.; Wade, C. G.; Waymouth, R. M.; Hedrick, J. L.; Rice, J. E. *J. Am. Chem. Soc.* **2008**, *130*, 6749−6754. (b) Simon, L.; Goodman, J. M. *J. Org. Chem.* **2007**, *72*, 9656−9662.

(9) Hammar, P.; Ghobril, C.; Antheaume, C.; Wagner, A.; Baati, R.; Himo, F. *J. Org. Chem.* **2010**, *75*, 4728−4736.

(10) (a) Gros, P.; Leperchec, P.; Senet, J. P. *J. Org. Chem.* **1994**, *59*, 4925−4930. (b) Li, H.; Wu, J.; Brunel, S.; Monnet, C.; Baudry, R.; LePerchec, P. *Ind. Eng. Chem. Res.* **2005**, *44*, 8641−8643. (c) Foulon, F.; Fixari, B.; Picq, D.; LePerchec, P. *Tetrahedron Lett.* **1997**, *38*, 3387−3390.

(11) (a) Soria, D. B.; Grundy, J.; Coles, M. P.; Hitchcock, P. B. *J. Organomet. Chem.* **2005**, *690*, 2278−2284. (b) Wild, U.; Roquette, P.; Kaifer, E.; Mautz, J.; Hubner, O.; Wadepohl, H.; Himmel, H. J. *Eur. J. Inorg. Chem.* **2008**, 1248−1257. (c) Huczynski, A.; Pospieszny, T.; Ratajczak-Sitarz, M.; Katrusiak, A.; Brzezinski, B. *J. Mol. Struct.* **2008**, *875*, 501−508. (d) Schulenberg, N.; Litters, S.; Kaifer, E.; Himmel, H.-J. *Eur. J. Inorg. Chem.* **2011**, 2657−2667.

(12) Leow, D.; Lin, S.; Chittimalla, S. K.; Fu, X.; Tan, C.-H. *Angew. Chem., Int. Ed.* **2008**, *47*, 5641−5645.

(13) Zhao, Y.; Truhlar, D. G. *Theor. Chem. Acc.* **2008**, *120*, 215−241. (b) Zhao, Y.; Truhlar, D. G. *Acc. Chem. Res.* **2008**, *41*, 157−167.

(14) Yang, H.; Wong, M. W. *J. Org. Chem.* **2011**, *76*, 7399−7405.

(15) Marenich, A. V.; Cramer, C. J.; Truhlar, D. G. *J. Phys. Chem. B* **2009**, *113*, 6378−6396.

(16) Reed, A. E.; Curtiss, L. A.; Weinhold, F. *Chem. Rev.* **1988**, *88*, 899−926.

(17) Frisch, M. J.; Trucks, G. W.; Schlegel, H. B.; Scuseria, G. E.; Robb, M. A.; Cheeseman, J. R.; Scalmani, G.; Barone, V.; Mennucci, B.; Petersson, G. A.; Nakatsuji, H.; Caricato, M.; Li, X.; Hratchian, H. P.; Izmaylov, A. F.; Bloino, J.; Zheng, G.; Sonnenberg, J. L.; Hada, M.; Ehara, M.; Toyota, K.; Fukuda, R.; Hasegawa, J.; Ishida, M.; Nakajima, T.; Honda, Y.; Kitao, O.; Nakai, H.; Vreven, T.; Montgomery, J. A., Jr.; Peralta, J. E.; Ogliaro, F.; Bearpark, M.; Heyd, J. J.; Brothers, E.; Kudin, K. N.; Staroverov, V. N.; Kobayashi, R.; Normand, J.; Raghavachari, K.; Rendell, A.; Burant, J. C.; Iyengar, S. S.; Tomasi, J.; Cossi, M.; Rega, N.; Millam, J. M.; Klene, M.; Knox, J. E.; Cross, J. B.; Bakken, V.; Adamo, C.; Jaramillo, J.; Gomperts, R.; Stratmann, R. E.; Yazyev, O.; Austin, A. J.; Cammi, R.; Pomelli, C.; Ochterski, J. W.; Martin, R. L.; Morokuma, K.; Zakrzewski, V. G.; Voth, G. A.; Salvador, P.; Dannenberg, J. J.; Dapprich, S.; Daniels, A. D.; Farkas, Ö.; Foresman, J. B.; Ortiz, J. V.; Cioslowski, J.; Fox, D. J. *Gaussian 09*, Revision A.02; Gaussian, Inc., Wallingford CT, 2009.

(18) (a) Kozuch, S.; Shaik, S. *J. Am. Chem. Soc.* **2006**, *128*, 3355−3365. (b) Kozuch, S.; Shaik, S. *Acc. Chem. Res.* **2010**, *44*, 101−110.

(19) (a) Allen, F. H. *Acta Crystallogr., Sect. B: Struct. Sci.* **2002**, *58*, 380−388. (b) Allen, F. H.; Motherwell, W. D. S. *Acta Crystallogr., Sect. B: Struct. Sci.* **2002**, *58*, 407−422.

(20) Khalaf, M. S.; Oakley, S. H; Coles, M. P.; Hitchcock, P. B. *CrystEngComm* **2008**, *10*, 1653−1661.

(21) Garrido, G.; Koort, E.; Rafols, C.; Bosch, E.; Rodima, T.; Leito, I.; Roses, M. *J. Org. Chem.* **2006**, *71*, 9062−9067.

(22) (a) Kozuch, S.; Shaik, S. *J. Phys. Chem. A* **2008**, *112*, 6032−6041. (b) Uhe, A.; Kozuch, S.; Shaik, S. *J. Comput. Chem.* **2011**, *32*, 978−985.

(23) (a) Becke, A. D. *J. Chem. Phys.* **1993**, *98*, 5648−5652. (b) Lee, C.; Yang, W.; Parr, R. G. *Phys. Rev. B* **1988**, *37*, 785−789.

(24) Perdew, J. P.; Burke; Ernzerhof, K. M. *Phys. Rev. Lett.* **1996**, *77*, 3865−3868.

(25) Grimme, S. *J. Comput. Chem.* **2006**, *27*, 1787−1799.

(26) Chai, J. D.; Head-Gordon, M. *Phys. Chem. Chem. Phys.* **2008**, *10*, 6615−6620.